

Article

Laser Surface Nitriding of Ti–6Al–4V Alloy in Nitrogen–Argon Atmospheres

Guang Li ^{1,2,3}, Xiaochun Yao ² , Richard James Wood ³, Jinchang Guo ² and Yu Shi ^{2,*}

¹ State Key Lab for Strength and Vibration of Mechanical Structures, Department of Engineering Mechanics, Xi'an Jiaotong University, Xi'an 710049, China; lg_xian@126.com

² State Key Laboratory of Advanced Processing and Recycling of Non-ferrous Metal, Lanzhou University of Technology, Lanzhou 730050, China; yaoxc1050@163.com (X.Y.); guojinchang2008@163.com (J.G.)

³ Centre for Applied Dynamics Research, School of Engineering, University of Aberdeen, Aberdeen AB24 3UE, UK; richard.wood1@abdn.ac.uk

* Correspondence: shiyu@lut.cn; Tel.: +86-931-2976-702

Received: 31 October 2019; Accepted: 9 October 2020; Published: 21 October 2020



Abstract: Surface-nitrided layers of Ti–6Al–4V alloy were fabricated using a diode laser in pure and mixed gas atmospheres of nitrogen and argon. The surface morphology, microstructure, hardness, and cracks of the nitrided layers were investigated. In all gas atmospheres, the layers showed smooth and humped regions, and consisted of planar nitrogen titanium (TiN), dendrites, and acicular martensite. The surface roughness was improved dramatically as the nitrogen concentration of the atmosphere was diluted with argon. Overall, the hardness of the nitrided layer was greatest for pure nitrogen and it tended to decrease as the concentration of argon in the atmosphere increased. However, the hardness of the layer for pure nitrogen also decreased rapidly, from the surface to matrix, in comparison to the diluted nitrogen atmospheres. It was shown that the number and size of dendrites, which determine hardness, are controlled by the nitrogen concentration. The dendrites of the nitrided layer were denser and smaller in a pure nitrogen atmosphere, than in diluted nitrogen atmospheres. Longitudinal and transverse cracks were observed in the nitrided layers. These two types of cracks were decreased or even eliminated as the argon concentration of the nitrogen–argon atmosphere was increased. Therefore, by diluting the nitrogen atmosphere with argon, the nitrided layer properties, in terms of surface roughness and cracks, can be improved, but this may also cause a reduction in the layer hardness.

Keywords: laser surface nitriding; Ti–6Al–4V alloy; surface morphology; hardness; cracks

1. Introduction

Commercially pure titanium and titanium alloys are receiving increased attention due to their high strength (to low weight) properties, high corrosion resistance, structural stability (at moderate or low temperatures), and some more unique characteristics (e.g., superconductivity and memory function) [1–3]. These metals are utilized in the aerospace, chemical and bio-medical, maritime, and military industries. They usually function as structural materials; however, due to the intrinsic low hardness and poor wear resistance of titanium (and its alloys) in conditions of friction and contact loads, their applications in engineering can be limited [3–7]. Thus, it is necessary to determine methods for the improvement of their hardness and wear resistance.

Attempts have been made to tailor the hardness and wear resistance of pure titanium and its alloys by a method of fabrication that involves titanium nitride embedded in the substrate. Ion implantation, physical vapor deposition (PVD), chemical vapor deposition (CVD), and salt-bath nitriding have also

been used to improve surface properties. However, the requirement for the whole work piece to be heated at high temperature can lead to large shape deformations. Furthermore, long processing cycles, the use of thin nitrated layers, and low combination strength can result in stripping between the nitrated layers and substrate during fabrication. These problems can be addressed by laser gas nitriding of the substrate whilst it is in a molten state. Laser gas nitriding as a fabrication technique, and in comparison to traditional methods, is characterized by reduced substrate deformation, stronger metallurgical zones, shorter fabrication times, and the ability to control the microstructure. It is well-documented in the literature that laser gas nitriding can modify the hardness and wear resistance of titanium and its alloys [8–10]. The purpose of laser gas nitriding in a nitrogen environment is to generate modified layers with greater hardness, increased wear resistance, and layers that are free from metallurgical defects. However, the major issues associated with laser gas nitriding are the problems of cracks in the nitride layers and their surface roughness, which dramatically decrease the fatigue life of fabricated components and materials, thus shortening their working life [1,11]. Although cracks in a single track can be eliminated by optimizing processing parameters, overlapping tracks are often required in engineering applications, which tend to develop network-interlaced cracks. Moreover, pores in the edges of nitriding tracks increase the surface roughness of overlapping nitrated layers.

This paper focused on diode laser fabrication of nitrated layers that are both free from cracks and have smooth surface morphology. The reaction rate of a nitrogen and titanium substrate can be decreased by introducing argon into a nitrogen atmosphere, resulting in a reduced amount of titanium nitride. The influence of this change in reaction rate on the surface morphology, hardness, depth of layers, microstructure, and cracks of the nitrated layers were investigated.

2. Materials and Methods

Commercially annealed Ti–6Al–4V alloy was used in this study. Its microstructure consisted of a hexagonal close-packed α phase mixed with some body-centered cubic β phase, as previously determined [11]. A sheet with a 120 mm diameter and 8 mm thickness was used as the treated substrate.

Prior to laser gas nitriding, the surface of the substrate was ground with 400-grade paper to remove oxides and other contaminants, and was then degreased with acetone. A schematic diagram of the diode laser gas nitriding process is shown in Figure 1. Laser gas nitriding was conducted in pure and different mixed atmospheres of nitrogen and argon, the concentrations of which were controlled via a self-developed annular gas delivery nozzle. A high-pressure zone of nitrogen and/or argon was generated at, and blocked by, the surface of the substrate as the gas was delivered. The diffusion of the gas from this high-pressure zone isolated the surrounding atmosphere and prevented oxidation during laser gas nitriding. The laser was fixed at a 10-degree angle (to the vertical) to prevent laser reflection damage.

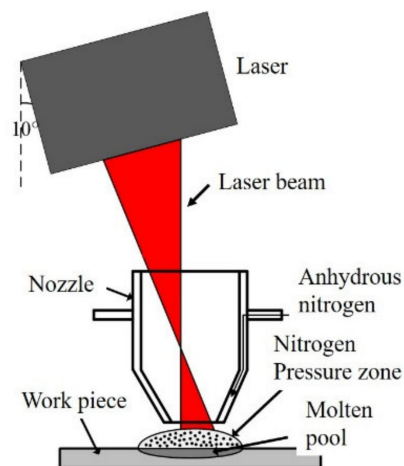


Figure 1. Schematic diagram of the laser gas nitriding process.

Initial tests showed that the optimal parameters for experiments were: laser power of 1200 W; movement speed of substrate, 180 mm/min; spot size of the laser of $2 \times 4 \text{ mm}^2$; gas flow of 33 L/min; and distance between substrate and nozzle of 4 mm. These parameters were applied to all experiments. The concentration of nitrogen (in the presence of argon) was varied from 10% to 100%; for example, at 10% nitrogen, the atmosphere was 10% nitrogen and 90% argon, at 100% nitrogen, the atmosphere was pure nitrogen.

Based on the above parameters, experiments were performed to produce different tracks on the surface of the titanium alloy. The diode laser emitted near infrared radiation at a wavelength of 976 nm and its energy distribution was trapezoidal. Tracks were cut into the Ti-6Al-4V alloy specimens ($20 \times 10 \times 8 \text{ mm}^3$) using a wire cutting machine across the nitriding process direction. Cross sections of nitrided layers were ground and polished by metallographic techniques and were then etched chemically in a solution of 3 mL of HF, 5 mL of HNO_3 , and 100 mL of H_2O for 15 s. The specimens were then cleaned by ultrasonic cleaners. An optical microscope and scanning electron microscope (SEM, FEI Company, Hillsboro, OR, USA) were used to determine the surface topography and microstructure. Microhardness was measured by a HV-1000 microhardness tester (ZhongYi, Shanghai, China) using a 1000 g load for 15 s on polished and etched sections of the nitrided layers. The area fraction of the dendrites in the cross section was calculated with ImageJ (PC) software (v1.8.0).

3. Results and Discussion

3.1. Surface Morphology of the Layers

Nitrided layer tracks, fabricated in pure and different mixed gas atmospheres of nitrogen and argon, were studied. Figure 2 shows the surface morphology of one track nitrided in a gas atmosphere of 80% nitrogen and 20% argon. The direction of laser motion is indicated by the black arrow (Figure 2a). To highlight the surface characteristics of the nitrided layer, the surface image was labeled with Area A and Area B, which are shown in more detail in Figure 2b,c respectively.

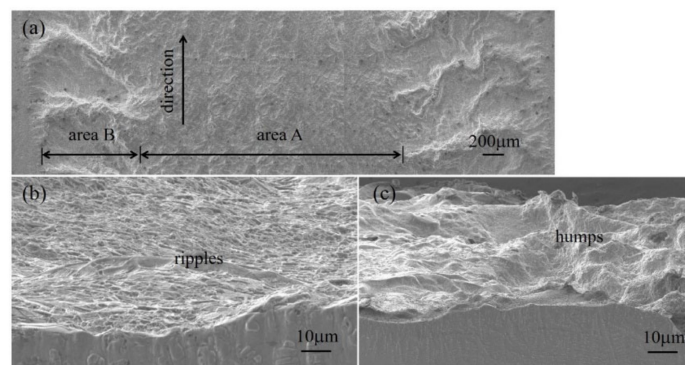


Figure 2. Surface morphology of one track nitrided in a gas atmosphere of 80% nitrogen and 20% argon. (a) Scanning electron microscope (SEM) image of the surface, and at higher magnification (b) Area A and (c) Area B.

Area A shows smoother surface characteristics, in comparison to Area B, and appeared more golden in color. The intensity of surface color is known to be positively correlated with higher nitrogen content of the layer, as previously observed by others. The convection strength reduces when the nitrogen concentration of the nitrogen–argon gas atmosphere varied from 91% to 10%. This is due to a reduction in nitrogen gas involved in the reaction, which reduces the temperature of the pool. Here, the amount of titanium nitride (which has a high melting point) decreases, consequently resulting in a molten pool of lower viscosity. The gas flow from the annular nozzle then causes turbulence in the molten pool surface, and a ripple structure is formed (Figure 2b). These convection-based ripple

effects do not occur in pure 100% nitrogen atmospheres or in atmospheres with less than 5% nitrogen, indicating that the structure can be drastically affected.

Area B is the transition region near the fusion line between the substrate and the nitrified tracks. It shows the concentrated regions of craters and humps (Figure 2a,c). The humps are thought to correspond to nitrogen-rich cells, and the craters to the titanium-rich cellular region, as previously observed [12].

The volume of the molten pool increases as the laser beam irradiates the substrate, which then also influences the surface tension of the pool. These effects control the flow of the metal fluid in the molten pool by Marangoni convection. Based on the phase diagrams of Ti–Al, Ti–V, Ti–Fe, and Ti–N, the dissolution of elements Al, V, and Fe causes decreases in the melting point of the titanium solutions. However, nitrogen (N) causes the melting point of titanium solution to rise. In the process of laser gas nitriding, a titanium solution absorbs a large amount of nitrogen, and the melting point rises more than 1668 °C. Here, strong convection leads to a nitrogen-containing melt overflow from the edge of the molten pool. It nucleates and solidifies immediately upon contact with the low-temperature un-melted substrate, and the solidification front has a cellular structure (Figure 2c). The cellular structure of the humped region, which represents the trailing edge of the molten pool, has been observed previously and can be explained by the Cline and Anthony model [13].

The surface roughness of the nitrified layer improved dramatically (becoming smoother) with a gas atmosphere of 5% nitrogen and 95% argon. Figure 3 shows the surface roughness (R_a) of the nitrified layers obtained for gas atmospheres of 100%, 80%, and 5% nitrogen (in argon) at positions along the surface of the layer. Compared with a maximum roughness depth (R_{max}) of 95 μm in the pure 100% nitrogen atmosphere (blue line), the maximum obtained in the 5% nitrogen and 95% argon atmosphere (red line) was reduced by at least four times to 23 μm (Figure 3). This depth meets the demands of several engineering applications. Thus, the surface roughness of the layer can be improved significantly by diluting the nitrogen atmosphere with argon.

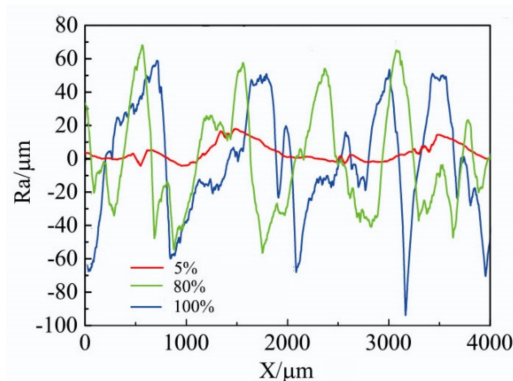


Figure 3. Roughness curves of the nitrified layers obtained in pure nitrogen (100%) (blue line), 80% nitrogen, and 20% argon (green line), and 5% nitrogen and 95% argon (red line) gas atmospheres.

3.2. Hardness of the Layers

The hardness profiles, along the cross section of the nitrified layers, showed that the surface hardness reached a maximum value in the pure (100%) nitrogen atmosphere (Figure 4). This is because, compared with the mixed nitrogen and argon atmospheres, the amount of titanium nitride in the nitrified layer increased. However, the hardness gradient of the nitrified layer, from the surface to the substrate, in the pure nitrogen atmosphere was steeper than that in the dilute nitrogen–argon atmospheres. The amount of nitrogen in the molten pool determines the pool temperature, which then determines the dissolution and diffusion of nitrogen into the pool, therefore, there is a nitrogen concentration gradient in the depth direction (surface to matrix) of the nitrified layer, as observed previously [14].

Thus, the hardness values at different positions along the nitrated layer are dependent on the nitrogen gas concentration of the atmosphere.

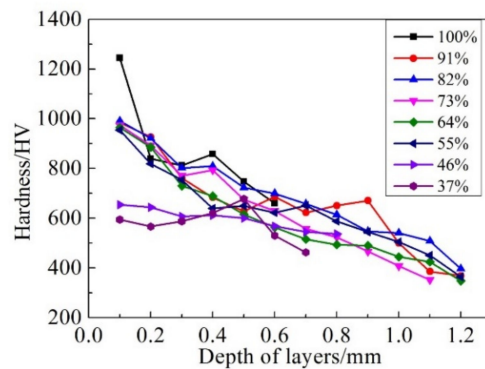


Figure 4. Hardness (HV) curves of the nitrated layer cross section in different nitrogen–argon gas atmospheres. The percentages represent the amount of nitrogen in the atmosphere; for example, 100% is pure nitrogen, and 37% is 37% nitrogen and 63% argon.

Energy spectrum curves of energy dispersive X-ray spectroscopy (EDX) point scanning on the cross section of the nitrated layer are shown in Figure 5. Positions 1 and 2 were located on dendrites of different depths (Position 2 was deeper than Position 1), and Position 3 was located on the structure between dendrites. The results showed that the nitrogen content between the dendrites was significantly smaller than that of the dendrites. The nitrogen content of the dendrites also decreased as the depth of the nitrated layer increased (Figure 5b,c).

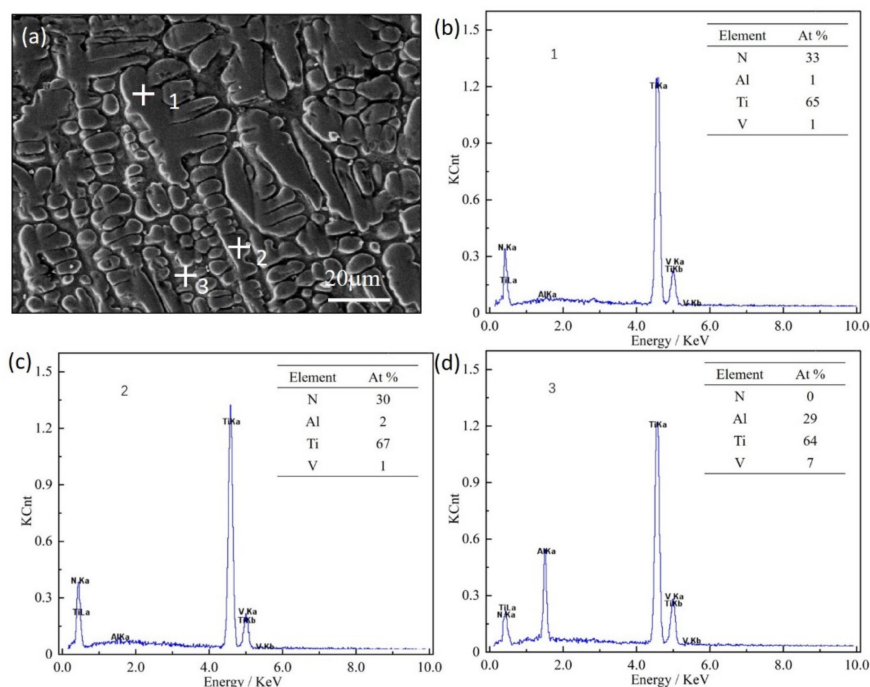


Figure 5. The energy spectrum curves of EDX point scanning. (a) SEM image of the cross section of the nitrated layer showing Positions 1, 2, and 3. (b) The energy spectrum curves of Position 1. (c) The energy spectrum curves of Position 2. (d) The energy spectrum curves of Position 3.

Overall, the surface hardness decreased dramatically when the amount of nitrogen in the nitrogen–argon atmosphere was less than 50% (Figure 4). There are at least three reasons for this: first, nitriding occurs through a process of nitrogen diffusion, hence, nitrogen has a gradient distribution,

and the amount of titanium nitride and phase type vary along the depth of the nitrified layer [15]; second, the thin planar TiN on the layer surface, and the dense titanium nitride underneath it, restricts nitrogen diffusion through the surface and into the bottom of the molten pool, so the nitrogen content in the molten pool decreases; and finally, the nitrogen concentration at the surface of the molten pool is influenced by the concentration of nitrogen present so that the amount of TiN_x in that region is changed [15]. Thus, it follows that laser gas nitriding in a nitrogen–argon atmosphere (as opposed to purely nitrogen) is at the expense of decreasing the hardness of the layer. For example, the surface microhardness of the nitrified layer is around 600 HV in 5% nitrogen and 95% argon, but 1240 HV in pure (100%) nitrogen.

The relationship between nitrogen content and dendrite area fraction in the cross section of the nitrified layer is shown in Figure 6. The area fraction of dendrites (titanium nitride) decreases with a decrease in the amount of nitrogen present in the nitrogen–argon atmosphere. Then, the hardness of the cross-section of the nitrified layer is positively correlated with the area fraction of dendrites (Figures 4 and 6). Previous authors [12] have determined the amount of nitrogen absorbed in the nitrified layer by weighing nitrified tracks. The results showed that the weight decreased by about 60% when the nitrogen concentration decreased by 11%.

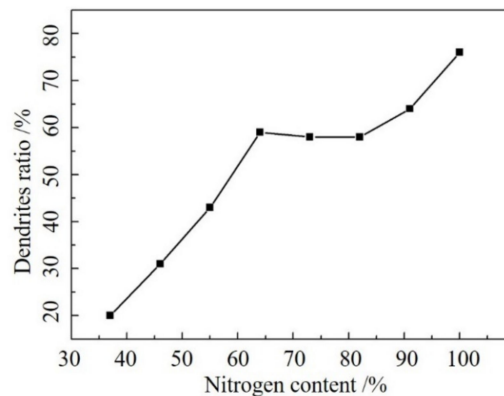


Figure 6. The relationship between the dendrite area fraction (in the cross section) and the nitrogen content of the nitrogen–argon gas atmosphere. When the nitrogen content of the nitrogen–argon atmosphere was less than 37%, the hardness curves were not plotted because the depth of the dendrites was less than 0.3 mm, and the microhardness was small.

The nitrogen content in the mixed nitrogen–argon atmosphere influences the dissolution and diffusion of nitrogen into the molten pool, so the subsequent concentration of titanium nitride in the pool changes, resulting in variable hardness values. Figure 7 shows the SEM images of the nitrified layer in pure (100%) nitrogen atmosphere, and an atmosphere of 64% nitrogen and 36% argon. The nitrified layer showed different morphologies and sized dendrites as the nitrogen concentration changes, which then influenced the hardness value. The dendrites of the nitrified layer were denser and smaller in a pure 100% nitrogen atmosphere, than in the 64% nitrogen (36% argon) atmosphere. The hardness tended to increase as the dendrite density and size increased. Therefore, the area fraction, size, and morphology of the dendrites have a dominant influence on the hardness, which are all influenced by the gas atmosphere.

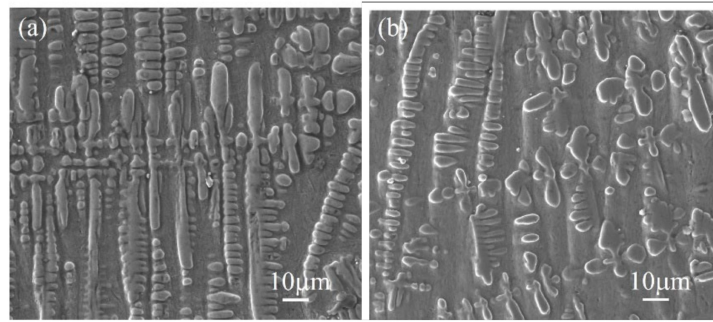


Figure 7. SEM images of the nitrided layer for different amounts of nitrogen in the nitrogen–argon atmosphere: (a) 100% nitrogen atmosphere, (b) 64% nitrogen and 36% argon atmosphere.

3.3. Microstructure of the Nitrided Layers

The fusion zone between the nitrided layer and the substrate was a completely metallurgical combination. The cross section of the nitrided sample consists of three parts: the nitrided layer, the heat-affected area, and the substrate (Figure 8). The heat-affected zone (Figure 8d) showed occasional acicular martensite. The nitrided layer was mainly composed of dendrites and acicular martensite in the pure (100%) nitrogen atmosphere. Then, as the nitrogen concentration of the nitrogen–argon atmosphere decreased, the dendrites in the nitrided layer reduced, and the amount of acicular martensite increased (Figure 9). The nitrided layer was composed of the thin planar layer and acicular martensite in an atmosphere of 5% nitrogen and 95% argon (Figure 9b). The thin planar layer only appeared on the surface of the nitrided layer in the diluted nitrogen atmosphere and not in a pure (100%) nitrogen atmosphere (not shown).

The surface XRD of the nitrided layer consisted of $\text{TiN}_{0.9}$ in a pure (100%) nitrogen atmosphere (Figure 10a). Then, for the thin planar layer, only TiN appeared in the 80% nitrogen (20% argon) atmosphere (Figure 10b). When the nitrogen concentration decreased further (5% nitrogen and 95% argon), the surface of the nitrided layers consisted of TiN and α' -Ti (Figure 10c).

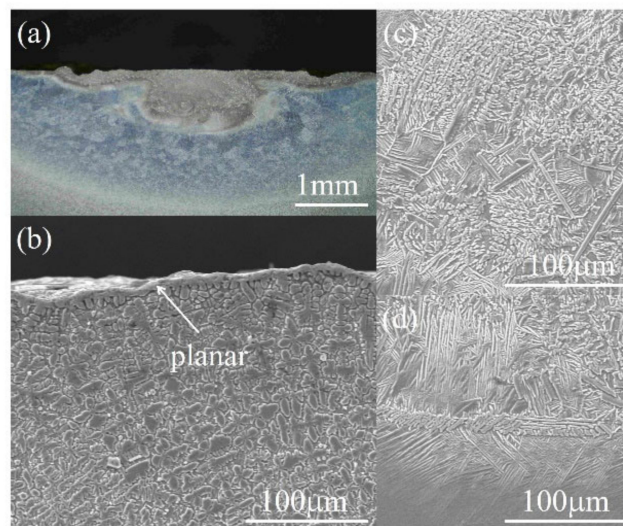


Figure 8. Optical microscope (a) and SEM image (b–d) of the nitrided layer in the 72% nitrogen and 28% argon atmosphere. (a) The cross section of the nitrided layer, (b) the microstructure of the nitrided layer, (c) the zone between the nitrided layer and the heat-affected area, and (d) the heat-affected area and matrix.

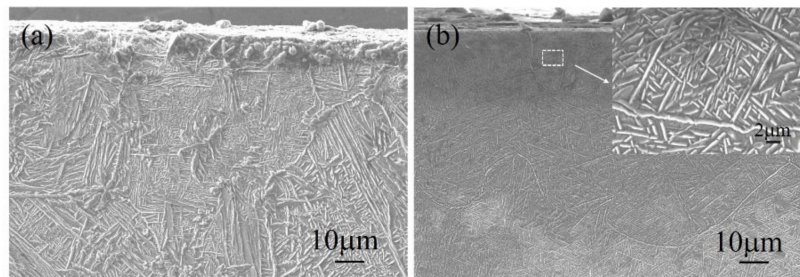


Figure 9. SEM image of the nitrided layer in different nitrogen–argon gas atmospheres: (a) 18% nitrogen and 82% argon, (b) 5% nitrogen and 95% argon.

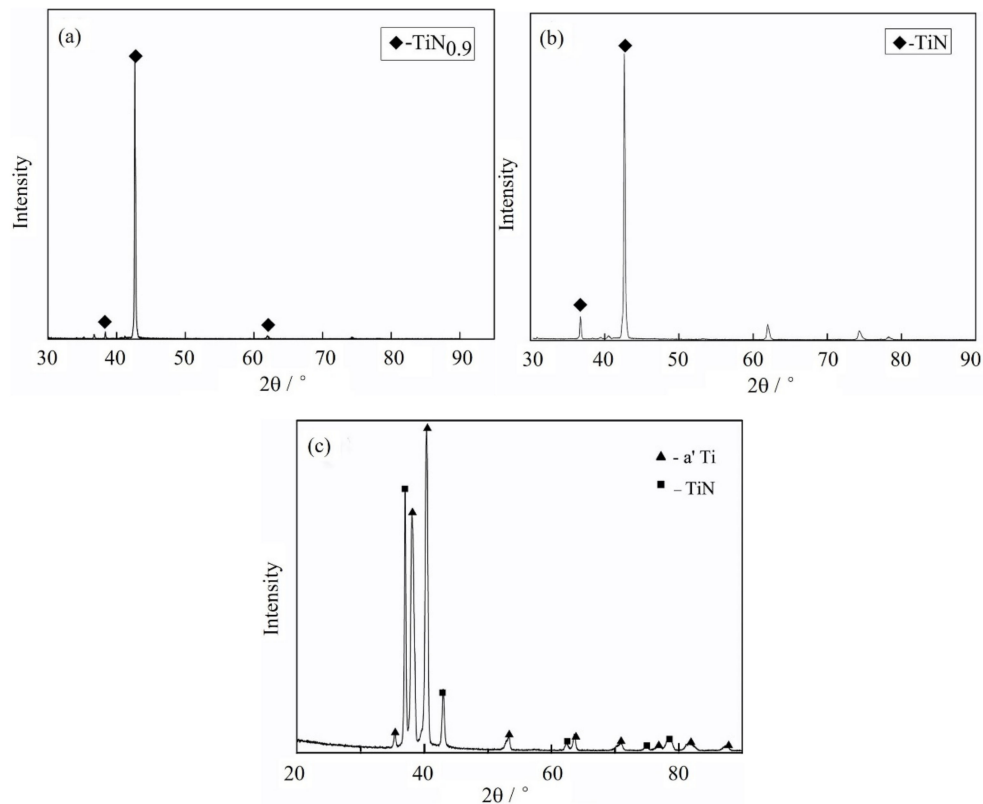


Figure 10. The surface XRD results of the nitrided layers obtained in different nitrogen content atmospheres; (a) pure (100%) nitrogen (100%), (b) 80% nitrogen and 20% argon, (c) 5% nitrogen and 95% argon.

The orientation of dendrites (Figure 8) was interesting, since the thermal gradient (G) was highest on the surface of the molten pool, and then decreased with depth, which influences the value for G/R (where R is radius of the molten pool). Thus, nitrogen absorbed into the molten pool caused the nitrogen concentration to be highest at the pool surface and then it decreased with depth (toward the bottom of the pool). Therefore, the surface reached the solubility limit for nitrogen in titanium more readily and solidified to form titanium nitride. Due to the nature of sub-cooling, the solidification front at the surface of the molten pool is not flat. There are solidifications that protrude, which lead to the development of dendrite structures. At the same time, another solidification front that is not nitrogen-rich proceeds from the bottom of the molten pool toward the surface, as observed by other authors [16]. Therefore, solidification mainly occurred from a solid solution of nitrogen in titanium, which showed acicular martensite (Figure 9).

Zhechena et al. [17] built up a simplified physical diffusion model for the formation and growth of the nitrated layer by the laser gas nitriding of pure titanium. The addition of alloy elements may cause a deviation of phases for the Ti–6Al–4V alloy. However, other elements in the titanium alloy are small in quantity and are usually dissolved in hcp α -Ti by formation of a substitutional solid solution. Thus, dramatic changes to the kinetics of formation and the phase compositions of the nitrated layers in the titanium alloy are not likely.

Based on the results of this work, and the conclusions of previous research on the microstructure and phase compositions of nitrated layers [12,15,18–20], the phase distribution of layers can be predicted (Figure 11). The XRD result of the nitrated surface illustrates that the thin planar layer on the surface was TiN, TiN_x was dendritic, and α' -Ti was acicular martensite, which may be a result of the β phase to martensitic α' -Ti transformation in a highly non-equilibrium condition. Phases in the nitrated layer may include hcp $\text{TiN}_{0.3}$ and Ti_2N , which form during the process of laser gas nitriding. The phase type also influences the hardness of the nitrated layer.

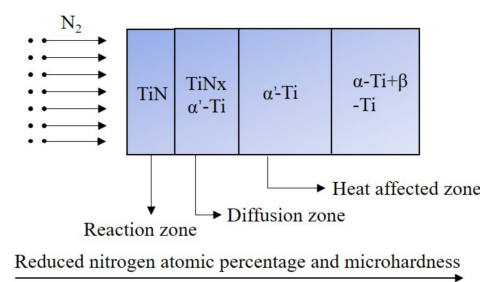


Figure 11. Schematic presentation of the phase distribution during the laser nitriding of titanium alloys.

The Heiple surface tension model can be used to explain formations in the microimages, which result from the molten pool (Figure 12). The surface tension gradient (with respect to temperature) of liquid titanium is negative, therefore shallow and wide molten pool formations are formed for the titanium alloy, and as previously observed [21].

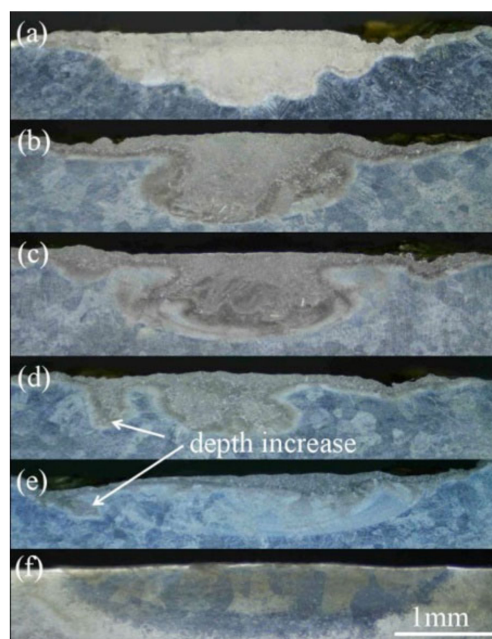


Figure 12. OM image of the cross section of the nitrated layers obtained for different nitrogen (in argon) concentrations: (a) 100% nitrogen, (b) 82% nitrogen 18% argon, (c) 64% nitrogen 36% argon, (d) 46% nitrogen 54% argon, (e) 18% nitrogen 82% argon, and (f) 5% nitrogen 95% argon.

The micrographs of the cross section of stringer beads (Figure 12) provide important information about the transport mechanism of nitrogen in the molten pool. When dendrites are produced in the nitrided layer, Marangoni convection dominates the molten pool dynamics in the pure (100%) nitrogen atmosphere. As argon is introduced into the gas flow, and the concentration of nitrogen is reduced, the fusion line becomes obscure (Figure 12b–d). In an atmosphere of 18% nitrogen and 82% argon, dendrites are limited to a very thin surface layer, and the fusion line completely disappears (Figure 12e). This shows that the transport mechanism of heat and mass changes from convection-dominated to diffusion-dominated when the nitrogen concentration decreases, and as observed by other authors [21]. However, the nitrided layer was entirely composed of acicular martensite (except for the thin planar layer of the surface) when the nitrogen concentration (of the nitrogen–argon atmosphere) was 5%, and convection dominated the molten pool dynamics. The depth of the nitrided layer was significantly deepened for the 46% and 18% nitrogen concentration atmospheres, as shown by the arrows in Figure 12d,e. This effect may have been caused by the annular nozzle used because the distance between the abrupt location of the molten depth and the center of the nitrided layer was equal to the radius of the annular nozzle, and the gas coming out of the annular nozzle deepened the depth of the molten pool.

3.4. Cracks of the Nitrided Layers

Longitudinal and transverse cracks were observed on the surface and the cross section of the nitrided layer in pure (100%) nitrogen (Figure 13a). The transverse cracks were perpendicular to the scanning direction and were approximately parallel to each other; here, they dominated the surface of the nitrided layer. Longitudinal cracks propagated from the surface nitrided layers down through the lower layers, but were then stopped at the heat-affected zone (Figure 13b,c). These cracks were not present in the overlapping tracks, which overlapped by 38%, under an atmosphere of 5% nitrogen and 95% argon (Figure 9). Here, the microstructure was composed of acicular structures and a thin planar layer.

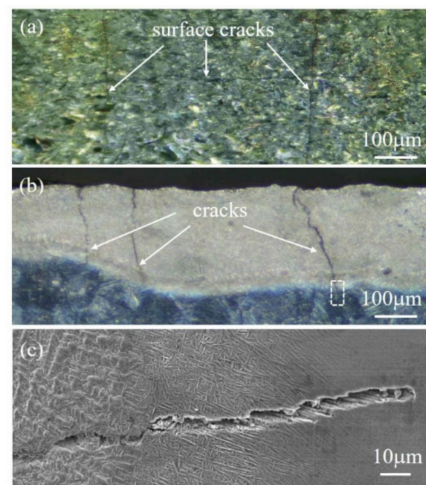


Figure 13. Cracking of the nitrided layer attained in the pure (100%) nitrogen atmosphere. (a) Surface cracking. (b) Cracking distribution through the layer. (c) Longitudinal cracking, the area illustrated by the dotted box in (b).

Due to intense local heating from the high-energy density diode laser, and the subsequent rapid cooling and addition of nitrogen, the laser nitriding process inevitably generates residual stress in the treated layer [22]. The stress is mainly caused by thermal and microstructure stress, and cracks occur when local residual stress exceeds the strength limit of the material. Cracks in the cross section of the nitrided layer can also originate from the process of cutting specimens. Microcracks between the

nitrided layers and the heat-affected zone may also be related to the inherent brittleness of titanium nitride [23].

4. Conclusions

The fabricated nitrided layers had both smooth and humped regions. As the concentration of nitrogen (of the nitrogen–argon atmosphere) decreased, the width of the smooth region tended to increase, and the surface became smoother. Therefore, the surface roughness of the nitrided layers was improved by diluting nitrogen with argon. For example, a maximum roughness depth of 95 μm was obtained in pure nitrogen, compared with 23 μm in the 5% nitrogen, 95% argon atmosphere. The hardness of the nitrided layer, overall, was greater in the pure (100%) nitrogen atmosphere compared with diluted nitrogen (in argon) atmospheres. However, there was also layer depth dependency and a steeper decrease in hardness for the layer in pure nitrogen as the depth of the layer increased. Laser gas nitriding by diluting nitrogen with argon is at the expense of decreasing the surface hardness. The surface microhardness of the (0.1 mm) nitrided layer was around 600 HV in the gas atmosphere of 5% nitrogen and 95% argon, whilst in pure (100%) nitrogen, it was 1240 HV. The cross section of the nitrided sample consisted of a nitrided layer, a heat-affected area, and a substrate. The nitrided layer had a thin planar TiN layer, dendrites, and acicular martensite. The thin planar TiN layer only appeared on the surface of the nitrided layer in a diluted nitrogen atmosphere, and not in pure 100% nitrogen. The number of dendrites was reduced, and the amount of acicular martensite was increased as the nitrogen composition of the nitrogen–argon atmosphere decreased. The surface of the nitrided layer appeared to contain both longitudinal and transversal cracks. Longitudinal cracks propagated from the surface of the nitrided layer down through the lower nitrided layers. These cracks were eliminated in single and overlapping tracks in the 5% nitrogen and 95% argon atmosphere.

Author Contributions: Conceptualization, G.L. and Y.S.; Validation, G.L., X.Y., R.J.W., J.G., and Y.S.; Investigation, G.L., X.Y., R.J.W., J.G., and Y.S.; Resources, G.L. and Y.S.; Data Curation, G.L. and Y.S.; Writing—original draft preparation, G.L. and X.Y.; Writing—review and editing, G.L., R.J.W., and J.G.; Supervision, G.L. and Y.S.; Project administration, G.L. and Y.S.; Funding acquisition, G.L. and Y.S. All authors have read and agreed to the published version of the manuscript.

Funding: This work was supported by NSFC (Nos. 52075235, 51961022, 51675256), China Postdoctoral Science Foundation (No. 2017M623153), and Basic Research of Gansu Province (No. 17JR5RA107).

Acknowledgments: Guang Li acknowledges support from the China Scholarship Council.

Conflicts of Interest: The authors declare no conflict of interest.

References

1. Man, H.C.; Bai, M.; Cheng, F.T. Laser diffusion nitriding of Ti–6Al–4V for improving hardness and wear resistance. *Appl. Surf. Sci.* **2011**, *258*, 436–441. [[CrossRef](#)]
2. Zhang, S.; Wu, W.T.; Wang, M.C.; Man, H.C. In-situ synthesis and wear performance of TiC particle reinforced composite coating on alloy Ti6Al4V. *Surf. Coat. Technol.* **2001**, *138*, 95–100. [[CrossRef](#)]
3. Biswas, A.; Li, L.; Chatterjee, U.K.; Manna, I.; Majumdar, J.D. Diode laser assisted surface nitriding of Ti–6Al–4V: Properties of the nitrided surface. *Metall. Mater. Trans. A* **2009**, *40*, 3031. [[CrossRef](#)]
4. Bansal, D.G.; Eryilmaz, O.L.; Blau, P.J. Surface engineering to improve the durability and lubricity of Ti–6Al–4V alloy. *Wear* **2011**, *271*, 2006–2015. [[CrossRef](#)]
5. Biswas, A.; Li, L.; Chatterjee, U.K.; Manna, I.; Pabi, S.K.; Majumdar, J.D. Mechanical and electrochemical properties of laser surface nitrided Ti–6Al–4V. *Scr. Mater.* **2008**, *59*, 239–242. [[CrossRef](#)]
6. Kaestner, P.; Olfe, J.; He, J.W.; Rie, K. Improvement in the load-bearing capacity and adhesion of TiC coatings on TiAl6V4 by duplex treatment. *Surf. Coat. Technol.* **2001**, *142*, 928–933. [[CrossRef](#)]
7. Santos, E.C.; Morita, M.; Shiomi, M.; Osakada, K.; Takahashi, M. Laser gas nitriding of pure titanium using CW and pulsed Nd: YAG lasers. *Surf. Coat. Technol.* **2006**, *201*, 1635–1642. [[CrossRef](#)]

8. Collin, M.; Coquerelle, G. Laser Nitriding and Carburizing of Ti–6Al–4V Titanium Alloy. In *The Laser vs. the Electron Beam in Welding, Cutting and Surface Treatment: State of the Art*; Reno: Englewood, NJ, USA, 1985; Volume 1, pp. 215–230.
9. Bell, T.; Bergmann, H.W.; Lanagan, J.; Morton, P.H.; Staines, A.M. Surface engineering of titanium with nitrogen. *Surf. Eng.* **1986**, *2*, 133–143. [[CrossRef](#)]
10. Mridha, S.; Baker, T.N. Crack-free hard surfaces produced by laser nitriding of commercial purity titanium. *Mater. Sci. Eng. A* **1994**, *188*, 229–239. [[CrossRef](#)]
11. Akarapu, R.; Nassar, A.R.; Copley, S.M.; Todd, J.A. Numerical model of a laser-sustained argon plasma. *J. Laser. Appl.* **2009**, *21*, 169–175. [[CrossRef](#)]
12. Kamat, A.M.; Copley, S.M.; Todd, J.A. Effect of processing parameters on microstructure during laser-sustained plasma (LSP) nitriding of commercially-pure titanium. *Acta Mater.* **2016**, *107*, 72–82. [[CrossRef](#)]
13. Cline, H.E.; Anthony, T.R. Heat treating and melting material with a scanning laser or electron beam. *J. Appl. Phys.* **1977**, *48*, 3895–3900. [[CrossRef](#)]
14. Fidel, A.F. Surface Hardening of Titanium with Laser. Master’s Thesis, Department of Mechanical Engineering, University of Garyounis, Benghazi, Libya, 2004.
15. Selamat, M.S.; Baker, T.N.; Watson, L.M. Study of the surface layer formed by the laser processing of Ti–6Al–4V alloy in a dilute nitrogen environment. *J. Mater. Process. Technol.* **2001**, *113*, 509–515. [[CrossRef](#)]
16. Kloosterman, A.B.; De Hosso, J.T.M. Microstructural characterization of laser nitrided titanium. *Scr. Metall. Mater.* **1995**, *33*, 567–573. [[CrossRef](#)]
17. Zhecheva, A.; Sha, W.; Malinov, S.; Long, A. Enhancing the microstructure and properties of titanium alloys through nitriding and other surface engineering methods. *Surf. Coat. Technol.* **2005**, *200*, 2192–2207. [[CrossRef](#)]
18. Majumdar, J.D. Laser gas alloying of Ti–6Al–4V. *Phys. Proc.* **2011**, *12*, 472–477. [[CrossRef](#)]
19. Abboud, J.H.; Fidel, A.F.; Benyounis, K.Y. Surface nitriding of Ti–6Al–4V alloy with a high power CO₂ laser. *Opt. Laser Technol.* **2008**, *40*, 405–414. [[CrossRef](#)]
20. Kaspar, J.; Bretschneider, J.; Jacob, S.; Bonß, S.; Winderlich, B.; Brenner, B. Microstructure, hardness and cavitation erosion behaviour of Ti–6Al–4V laser nitrided under different gas atmospheres. *Surf. Eng.* **2007**, *23*, 99–106. [[CrossRef](#)]
21. Heiple, C.R. Mechanism for minor element effect on GTA fusion zone geometry. *Weld. J.* **1982**, *61*, 97.
22. Pérez, M.G.; Harlan, N.R.; Zapiain, F.; Zubiri, F. Laser nitriding of an intermetallic TiAl alloy with a diode laser. *Surf. Coat. Technol.* **2006**, *200*, 5152–5159. [[CrossRef](#)]
23. Selvan, J.S.; Subramanian, K.; Nath, A.K.; Gogia, A.K.; Balamurugan, A.K.; Rajagopal, S. Hardness, microstructure and surface characterization of laser gas nitrided commercially pure titanium using high power CO₂ laser. *J. Mater. Eng. Perform.* **1998**, *7*, 647–655. [[CrossRef](#)]

Publisher’s Note: MDPI stays neutral with regard to jurisdictional claims in published maps and institutional affiliations.



© 2020 by the authors. Licensee MDPI, Basel, Switzerland. This article is an open access article distributed under the terms and conditions of the Creative Commons Attribution (CC BY) license (<http://creativecommons.org/licenses/by/4.0/>).